ADVANCED FUNCTIONAL MATERIALS
www.afm-journal.de

Materials Views
www.MaterialsViews.com

Origins of Low Quantum Efficiencies in Quantum Dot LEDs

*Deniz Bozyigit, Olesya Yarema, and Vanessa Wood**

The promise for next generation light-emitting device (LED) technologies is a major driver for research on nanocrystal quantum dots (QDs). The low efficiencies of current QD-LEDs are often attributed to luminescence quenching of charged QDs through Auger-processes. Although new QD chemistries successfully suppress Auger recombination, high performance QD-LEDs with these materials have yet to be demonstrated. Here, QD-LED performance is shown to be significantly limited by the electric field. Experimental field-dependent photoluminescence decay studies and tight-binding simulations are used to show that independent of charging, the electric field can strongly quench the luminescence of QD solids by reducing the electron and hole wavefunction overlap, thereby lowering the radiative recombination rate. Quantifying this effect for a series of CdSe/CdS QD solids reveals a strong dependence on the QD band structure, which enables the outline of clear design strategies for QD materials and device architectures to improve QD-LED performance.

1. Introduction

Colloidally synthesized semiconductor quantum dots (QDs) receive substantial attention as candidates for next-generation, low-cost light emitting devices (LEDs). The hopes for QD-based lighting and displays stem from the versatility of the colloidal synthesis technique and the excellent optical properties of QDs, including tunable optical bandgaps and near-unity photoluminescent (PL) quantum yield (QY). While the first demonstration of electroluminescence (EL) using QDs dates back to 1994,[1] the best reported external quantum efficiency (EQE) from QD-LEDs is 7.3%.[2] In order to improve the performance of QD-LEDs to the point of commercial relevance, a detailed understanding of the physical origins of these low EQE values is needed.

The EQE, which is defined as the ratio of the number of photons emitted from the device per second to the number of electrons injected into the device per second, depends on both the probability that an exciton is formed and the probability of an exciton being transformed into a photon (i.e., the luminescent QY). The large discrepancy between the QY of the emitters in solution and in solid state during device operation suggests that the low EQE values likely stem from inefficiencies in the radiative recombination of the excitons. In order to understand how device operation can effect the QY of the QD emitters, it is helpful to express the QY as:

$$QY = (1 - N)k_r\tau, \quad (1)$$

where k_r is the radiative exciton decay rate, τ is the exciton lifetime, and N is the fraction of QDs in a non-emitting state. Although τ is related to k_r, this dependence can be neglected in the case of low QYs where $\tau = (k_r + k_{nr})^{-1} \approx k_{nr}^{-1}$ such that the lifetime is a measure for the non-radiative recombination rate, k_{nr}. It is widely accepted that the radiative and non-radiative rates and the number of non-emitting QDs can be affected by some combination of charging of the QD thin film and the electric field present across the QD film during device operation (**Figure 1**a).

In LED structures where charge is injected in the QD thin film to achieve EL, a large fraction of QDs (N) can acquire a net charge. These charges can absorb the exciton energy by non-radiative Auger processes rendering the QD dark.[3] Surface states that can trap charge are particularly prevelant in QD solids where oxidation of the QDs or loss of passivating ligands occurs. These states can be reduced by coating the QD core with a shell[4] and selection of more stable ligands, but complete elimination of QD charging in LED structures is not feasible. Therefore, it was recently proposed that QDs with graded or reduced confinement potential should be employed to reduce Auger processes.[5] Charged CdSe/CdS core/shell QDs retain high QY even when singly or doubly charged .[6] Nonetheless, LEDs incorporating such alloyed and graded shell QD structures still show low EQE of around 0.15 %.[3,7]

This hints at the important role of the electric field in quenching the luminescent QY of QDs. Regardless of the QD-LED architecture, during operation of an LED, the QD active layer will experience electric fields between 0.5 MV cm^{-1} and 4 MV cm^{-1}.[3,7] We recently reported that electric fields >1 MV cm^{-1} strongly quench the QY in CdSe/ZnS QD solids.[8] This observation is in agreement with a number of reports on luminescence quenching by the electric field in measurements of single CdSe/ZnS QDs,[9–11] CdSe/ZnS nanocrystal rods,[12] and CdSe QD solids[13] and CdSe QD ensembles embedded in an insulating matrix.[14,15] Despite these studies, the mechanisms by which this field-driven luminescence quenching

D. Bozyigit, O. Yarema, Prof. V. Wood
Laboratory for Nanoelectronics
Department of Information Technology
and Electrical Engineering
Eidgenoessische Technische Hochschule Zurich
Zurich, Switzerland
E-mail: vwood@ethz.ch

DOI: 10.1002/adfm.201203191

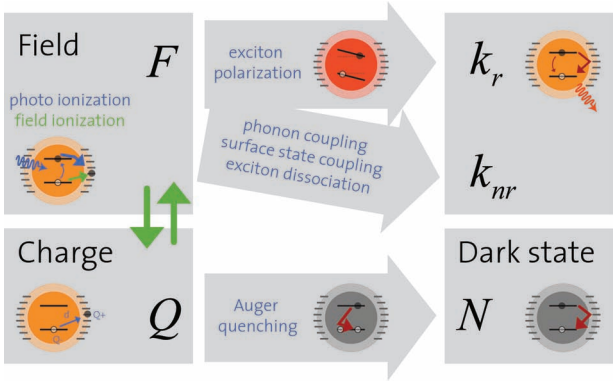

Figure 1. Schematic showing how electric field (F) and charge (Q) influence key parameters of QD luminescence: the radiative exciton decay rate (k_r), non-radiative exciton decay rate (k_{nr}), and the fraction of dark QDs (N). The middle column shows a variety of field and charge related processes that have been reported to affect the luminescence properties of QDs.

occurs are not understood, leaving no clear insight as to how QDs emitters should be designed to minimize field-induced luminescence quenching.

To this end, we develop a device structure that can be used to systematically investigate effect of electric field on the luminescent QY of QD solids. In standard QD-LEDs, it is difficult if not impossible to distinguish between luminescence quenching due to the applied field and quenching due to charging, since both processes occur simultaneously. We therefore turn to a capacitive structure shown in **Figure 2**a. In this structure, a multilayer

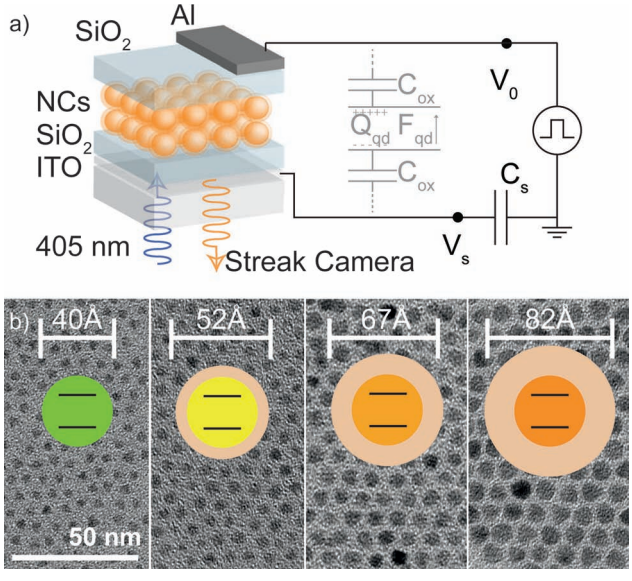

Figure 2. a) Experimental setup for the field-dependent PL lifetime measurements. A QD solid thin film capacitor is connected to a voltage pulse source. Measurement of the device voltage (V_0) and the sense capacitor voltage (V_s) enables calculation of the electric field across the QD film (F_{qd}) and the polarization charge (Q_{qd}) in the QD film. QDs are optically excited by a 405 nm ps-pulse laser and the PL response is collected through the ITO glass substrate. b) TEM images of the CdSe/CdS QDs used in this study.

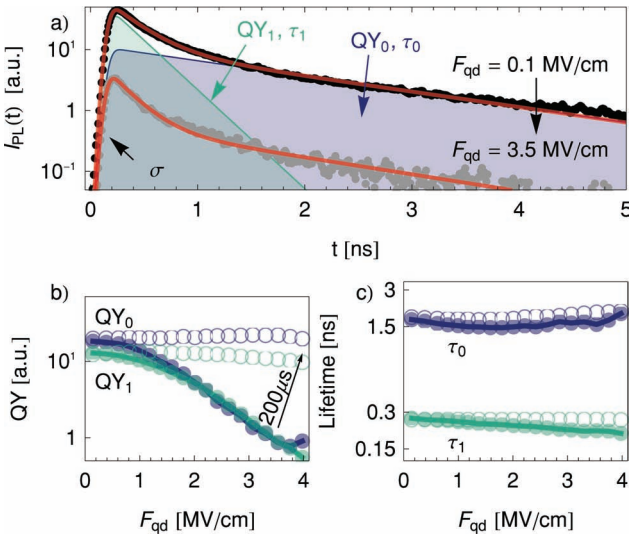

Figure 3. a) PL response of the QD solid under low field (black) and high field (gray). The PL decay is described well by two exponential components with amplitudes and time constants, QY_0, τ_0 (purple) and QY_1, τ_1 (green). The response can be fitted accurately (red) considering a finite system resolution (σ) using Equation (2). PL response is strongly quenched under high fields. b) Relative QY of both fluorescence components vs. the applied field (F_{qd}) (solid markers). After application of field, the QY fully recovers in <200 µs (open markers). c) Lifetimes of both fluorescence components (τ_0, τ_1) show only weak field-dependence, comparable to the measurement error.

of QDs is embedded between two SiO_2 dielectric thin films. As shown in Figure 2b, the QDs used in this study have 0, 6, 14, and 21 Å CdS shells synthesized on the same 40 Å CdSe cores according to the procedure described by Mahler.[16] The electric field is applied across the QD and SiO_2 sandwich between a bottom transparent indium tin oxide (ITO) and a top Aluminum electrode. This structure enables application of electric fields across the QD solid without charge injection from the electrodes. The absolute PL QY of the devices varies between samples but was in all cases <10%. By characterizing the capacitance of the SiO_2 and QD layers, we can calculate the field dropped across the QD layer (F_{qd}) for a given voltage applied to the device structure.

2. Results and Discussion

2.1. Measuring Field-Dependence of the Luminescence QY

We measure the time resolved photoluminescence (PL) response as a function of applied field. **Figure 3** shows the measurement results for a representative device incorporating QDs with a 14 Å CdS shell. The QDs are excited with a 405 nm ps-pulsed diode laser and their PL is collected with a streak camera. As shown in Figure 3a, the decay of PL intensity (I_{PL}) can be fit with a double exponential:

$$I_{PL}(t) = \left(\frac{QY_0}{\tau_0}e^{-t/\tau_0} + \frac{QY_1}{\tau_1}e^{-t/\tau_1}\right) g(t). \quad (2)$$

QY_i are the relative quantum yields and τ_i are the lifetimes for the two components, which can be extracted by a non-linear

curve fitting method. The time resolution of the complete system is modelled by a convolution with a gaussian response function $g(t)$, with a standard deviation of $\sigma = 43$ ps. The lifetimes we find are ≈2.0 ns and ≈0.2 ns, which is in agreement with previous measurement of with singly (X^-) and doubly (X^{2-}) charged exciton states,[17] respectively.

We generate an electric field across the QD film by applying voltage pulses 100 µs in duration to the device. The pulses alternate in polarity and have a duty cycle of 10%. In this way, we can achieve field strengths of up to 4 MV cm^{-1} across the QD layer without degrading the devices. The field in the QD film (F_{qd}) is determined during the experiment by measuring the voltages V_0 and V_s and using the equivalent circuit in Figure 2a as in ref. [8,18]. Performing the time resolved PL measurements during the voltage pulse we observe a strong quenching of the luminescence (Figure 3a, gray).

By varying the magnitude of the voltage pulse, we probe field values between 0 and 4 MV cm^{-1}. Two clear trends are observed as a function of F_{qd}. First, plotting both QY_0 and QY_1 vs. F_{qd} (Figure 3b, solid markers), we find that the relative QYs go down exponentially with increasing field to less than 10% of the initial value. Second, the lifetimes τ_0 and τ_1 do not change significantly (Figure 3c, solid markers).

We also repeat the experiment applying the same bias conditions, now measuring the PL lifetime 200 µs later, at which time the applied voltage is zero. The PL quenching effect disappears completely (Figure 3b, open markers). From this, we conclude that the luminescence quenching stems directly from the electric field and not from a secondary effect such as degradation or any long time scale change of the system state.

2.2. Implications of the Field-Independent Lifetime τ

The most intuitive picture to explain PL quenching under high fields is the dissociation of excitons, where the Coulombic bond of the electron hole pair is overcome by the force of the electric field and one of the charge carriers escapes from the QD. This process can be modelled by the electron overcoming an energy barrier by tunnelling or thermal excitation. This barrier would be reduced by the applied electric field and we would expect an exponential increase of the dissociation rate. This is in agreement with our observation that the relative QY drops exponentially with the electric field (Figure 3b).

However, exciton dissociation would provide an additional, non-radiative decay path for the exciton and therefore change its decay dynamics. An estimation of the field-dependence of the dissociation rate (k_{diss}) is given by the Onsager-Braun model,[19] which reduces in the limit of high fields to

$$k_{diss}(F_{qd})/k_{diss}(0) \approx \exp\sqrt{F_{qd}/F_0}, \quad (3)$$

where F_0 is a free parameter of the barrier. If exciton dissociation were to become the dominant decay mechanism at high fields, we would expect a strong reduction in the PL lifetime of the approximate form $\tau(F_{qd}) \approx k_{diss}^{-1}(F_{qd})$. As we observe no such dependence of τ, we can exclude exciton dissociation as the primary quenching mechanism. By the same arguments, our finding of a field-independent lifetime enables us to exclude other non-radiative processes, such as phonon-coupling,[9] or surface state coupling.[10]

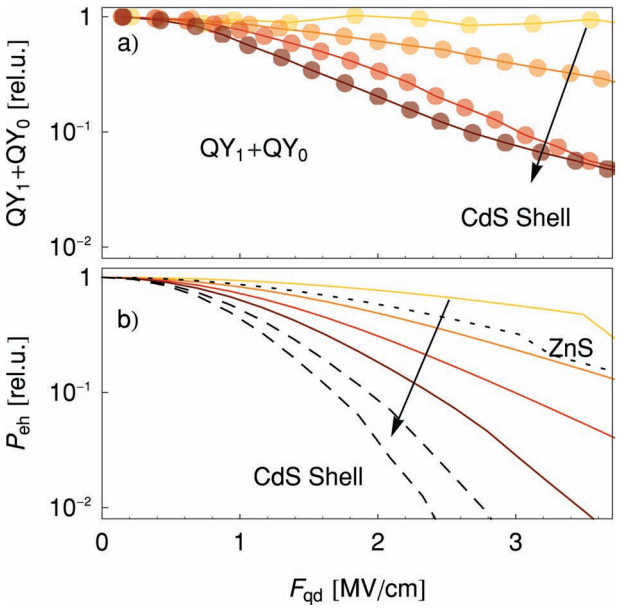

Figure 4. a) Relative QY vs. applied field (F_{qd}) for CdS shell thicknesses of 0 Å (yellow), 6 Å (orange), 14 Å (red), and 21 Å (brown). The dependence on the field is more pronounced for thicker shells. b) Optical matrix element (P_{eh}) of the lowest energy exciton, as determined by tight binding simulations for the experimentally assessed shell thicknesses (color coding as in (a)). As a comparison simulation results for thicker CdS shells (26 Å and 30 Å (dashed) and for a 21 Å ZnS shell are given (dotted).

This result is in agreement with the report of Leatherdale[20] from 2000 and our report[8] from 2012, which determine the field-driven exciton dissociation efficiency in weakly coupled QD solids to be on the order of 10^{-5} at 1 MV cm^{-1}. Although ref. [20] states that fluorescence quenching cannot be quantitatively explained by their observations, it was later assumed by Jarosz[13] in 2004 and Huang[11] in 2007 that exciton dissociation in QD solids approaches unit efficiency at high fields. Due to these reports, field-driven exciton dissociation is often incorrectly cited as the reason for field induced quenching in the community.

2.3. Field-Dependence of the Radiative Rate k_r

Since the decrease of the PL QY as a function of field cannot be explained by an increase in non-radiative processes, we perform the measurements described in Section 1.1 for different CdS shell thicknesses so that we can observe variations in the PL quenching as a function of the QD band structure. As shown in **Figure 4**a, the field-dependent quenching of the PL is enhanced in QDs with thicker CdS shells. To explain this effect, we assess the field-dependence of the radiative decay rate (k_r) in Equation (1). We consider that k_r is proportional to the optical matrix element (P_{eh}) of the electron and hole state and calculate:

$$k_r \propto P_{eh} = |\langle\psi_e|\,\vec{p}\,|\psi_h\rangle|^2, \quad (4)$$

where $|\psi_{e,h}\rangle$ are the electron and hole wavefunctions and $\vec{p}$ is the momentum operator.

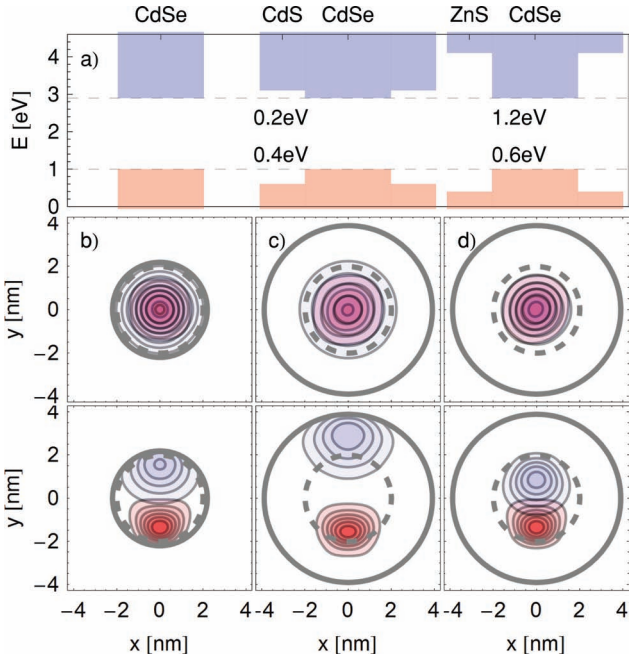

Figure 5. a) Schematic band structures for CdSe, CdSe/CdS, and CdSe/ZnS materials used in the simulations. The inset numbers provide the relative band offsets. b) Wavefunctions of electron (blue) and hole (red) for CdSe QD at F_{qd} = 0 MV cm^{-1} and 4 MV cm^{-1} (top, bottom). Spatial separation of the electron and hole can be observed. c,d) as before, but for CdSe/CdS and CdSe/ZnS QDs with 21 Å shells. In the CdSe/CdS QD, the reduced band offset of the conduction band (0.2 eV) allows a strong separation of the electron and hole.

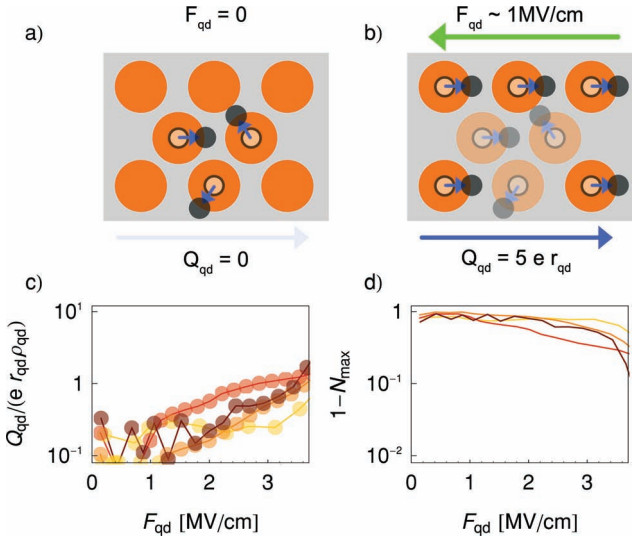

Figure 6. a) Small dipoles in s QD solid show typically no macroscopic polarization. b) Application of an electric field can induce additional dipoles. These dipoles are aligned with the field and result in a measurable polarization. c) Estimation of the upper bound for the number of field-induced dipoles per QD in the QD film based on the measurement of the polarization charge (Q_{qd}). The data is shown for QDs with CdS shell thicknesses of 0 Å (yellow), 6 Å (orange), 14 Å (red), and 21 Å (brown). d) Upper bound for the QY quenching through field-induced charging of QDs derived from data in (c) (same color coding).

The solutions are found using a quantum mechanical solver based on the empirical tight-binding model[21] and the material parameters of ref. [22,23]. **Figure 5** shows the lowest energy electron and hole wavefunctions for CdSe QDs with no or a 21 Å-thick CdS shell at 0 4 MV cm^{-1} 0 MV cm^{-1} and 4 MV cm^{-1}.

In comparison to the core only QDs (Figure 5b), the type-II band alignment in CdSe/CdS (Figure 5c) strongly reduces the confinement of the electron and allows it to penetrate the shell, in agreement with measurements in ref. [24]. In contrast, the hole stays confined due to the large valence band offset between CdSe and CdS. When a field is applied to the QD, the hole and electron wavefunctions separate spatially (Figure 5b,c, bottom), which reduces P_{eh} and therefore k_r. The separation of the electron and hole wavefunctions becomes even more pronounced for thicker shells due to the reduced confinement of the electron.

Indeed, plotting P_{eh} vs. F_{qd} in Figure 4b shows a weak field-dependence in the absence of a shell. With a CdS shell, P_{eh} develops a strong field-dependence, in quantitative agreement with the experimentally measured change of the QY. We conclude that the primary source for luminescence quenching in CdSe/CdS QDs is a reduction of the radiative rate k_r by the polarization of the exciton wavefunction by the electric field.

As a comparison, we perform the same simulations for ZnS shells (Figure 5d). The large energy offsets keep both the electron and the hole confined in the core. The field-dependence of P_{eh} for a ZnS shell plotted in Figure 4b (dotted line) is less pronounced than in the case of a CdS shell. Furthermore, for ZnS shells thicker than 10 Å, no change in the P_{eh} vs. F_{qd} relation is observed. At 4 MV cm^{-1}, we find a reduction of P_{eh} of 90%, which is consistent with our earlier results on CdSe/ZnS.[8]

2.4. Field-Induced QD Charging

In order to confirm that the field-dependent luminescence quenching we observe results from spatial separation of electron and hole wavefunction and not from field-induced charging of the QDs, we calculate the additional fraction (N) of QDs that may become charged (and therefore turn dark) due to the applied field. In our capacitive structure, the QD film is charge neutral and no additional charge is injected with increasing field. However, some percentage of QDs will be charged and not luminescence[17] due to local fluctuation of the charge.[9] As shown schematically in **Figure 6**a, this can occur for example when a valence band electron fills a trap state, leaving a hole.[17] This configuration of charge can be regarded as an elemental dipole (p_{qd}) with a length of the QD radius (r_{qd}) such that $p = er_{qd}$ where e is the elementary charge. Under no applied field, these dipoles are randomly oriented so that the net polarization charge (Q_{qd}) across the QD film is zero (Figure 6a). Application of an electrical field can align or induce more dipoles such that $Q_{qd} > 0$ (Figure 6b). Measuring Q_{qd} and assuming a configuration that would minimize the number of dipoles per QD (and therefore maximize the number of charged QDs), we can arrive at an upper bound for the additional number of charged QDs we create by applying an electric field.

To measure Q_{qd} as a function of field, we apply the same voltage pulses as in our measurement of the PL QY, but without

optically exciting the QD film. As charge is polarized in the QD film, it also accumulates on the sense capacitor and can be determined by recording the voltage drop across the sense capacitor. Using the equivalent circuit model from ref. [18], we can extract Q_{qd} (see Figure 6c and Supporting Information).

This measurement of Q_{qd} does not provide a detailed spatial map of the charge in the QD film; however, we can use it to estimate the maximum number (N_{max}) of QDs that become charged due to the applied electric field. Assuming that the macroscopic polarization charge (Q_{qd}) stems from elemental dipoles, the number of elemental dipoles per QD is given by $\frac{Q_{qd}}{er_{qd}\rho_{qd}}$, where ρ_{qd} is the volume density of QDs. We calculate ρ_{qd} by assuming close packing of the QDs and using dielectric measurements.[8] If we assume that the induced dipoles are randomly distributed, the maximum number of additional QDs occupied by a charge is:

$$N_{max} = 1 - \exp\left(-\frac{Q_{qd}}{er_{qd}\rho_{qd}}\right). \quad (5)$$

We compare the resulting estimation for the quenching effect due to field-induced charging ($1 - N_{max}$) (Figure 6d) to the measured decrease in QY (Figure 4a) and find that the estimated quenching due to charging is in all cases too small to explain the decrease in QY and does not follow the observed trend with CdS shell thickness. Since we chose a picture of charge distribution that overestimates the magnitude of quenching due to field-induced charging, we conclude that this effect can at most account for a fraction of the quenching of the QY.

3. Conclusion

In this work, we demonstrate that field-dependent luminescence lifetime measurements are a powerful method to investigate the physical processes relevant for luminescence in QD-LEDs. Additionally, the use of a capacitive structure enables us to suppress charge injection and to investigate the effect of the electric field in absence of mobile charge.

Our results on CdSe/CdS core-shell QDs show a strong quenching of the luminescence quantum yield (QY) under fields of 0.5–4 MV cm^{-1}. At the same time, the PL lifetime is only weakly field-dependent, which excludes many non-radiative processes as the source of the field-dependent quenching, most importantly exciton dissociation, phonon-coupling,[9] and surface state coupling .[10]

We use a combination of experiment and simulations to identify that field-dependence of the radiative rate (k_r) is the source of reduced QYs at high fields. This effect stems from the field-induced spatial separation of electron and hole wavefunctions, which is particularly pronounced in QD band structures with relaxed confinement potentials. Such relaxed confinement potentials occur predominantly in core/shell structures with type-II band alignments, where either the electron or the hole part of the exciton has the possibility to extend into the shell. However, our simulations show that the field-induced spatial separation still occurs even in QDs with a wide bandgap shell material, such as ZnS.

Our findings have two key consequences for the design of high performance QD-LEDs. First, QD-LED architectures must feature low operating fields (<0.5 MV cm^{-1}) in regions where QDs are located. Indeed, our results explain improved QD-LED performance in ref. [2] where the electric field in the QDs is minimized in forward bias by the inverted device structure, or in ref. [25] where efficiency was improved by moving QDs out of the high field interface regions in the LED.

Second, current trends in the development of QD band structures must be reconsidered. While CdSe/CdS giant shell QDs have largely eliminated quenching due to charging,[26–28] the reduction of the quantum confinement of the electrons introduces strong field-driven quenching. This can explain why recent demonstrations of QD-LEDs based on these materials have not achieved high efficiencies.[7] New QD chemistries must be formulated not only to decrease Auger-processes but also to retain large electron-hole overlap under applied electric fields.

4. Experimental Section

CdSe QD Synthesis: The synthesis of CdSe cores is reported in ref. [29,30]. Here, 821.8 mg cadmium oxide (6.4 mmol), 46 g hexadecylamine (0.19 mol), 18.6 g tri-n-octylphosphine oxide (48 mmol), and 3.2 g dodecylphosphonic acid (12.8 mmol) were loaded in a 259 mL four-neck flask and heated under vacuum at 120 °C to dry the solution. Next, under N_2 flux, the temperature was increased to 329 °C and held for 30 min until the precursor solution becomes clear. At 270 °C, an injection mixture, containing 0.2 M solution of TOPSe and 0.5 mL of diphenylphosphine, was added swiftly to the reaction solution. CdSe QDs formed immediately after injection, inducing a color change to bright yellow. After 4 min of nanocrystal growth at 250 °C, the reaction solution was cooled to room temperature. Anhydrous toluene (20 mL) was added at 60 °C to prevent solidification of the reaction mixture. The nanocrystals were isolated by addition of 100 mL toluene and a polar ethanol/methanol (4/1) mixture.

The CdS shell synthesis was performed as described in ref. [16]. Oleylamine (4 mL), octadecene (8 mL), and CdSe core solution (0.5 mL with 40 mg mL^{-1} in toluene) were loaded into a three-neck flask. The toluene was then removed under reduced pressure at 70 °C for 30 min. Cadmium oleate stock solution (0.1 M, 0.56 mL)[16] was added to the mixture, after which the temperature is increased to 230 °C. The same quantity of sulfur stock solution (0.1 M in octadecene)[16] was introduced dropwise 10 min later. To obtain CdS shells of a specific thickness, the cadmium and sulfur stock solutions were added sequentially every 10 min with the flask kept at 240 °C. The volumes of further injection solutions were 0.92, 1.30, 1.74, 2.26 mL, corresponding to the increasing shell size. The reaction mixture was quenched 20 min after the last cadmium injection. CdSe/CdS QDs were purified by adding 160 mL of ethanol and redispersed in chloroform. The origin of the chemicals used were as follows: cadmium (II) oxide (99.999%), selenium powder (99.99%), tri-n-octylphosphine (TOP, 97%) were purchased from Strem Chemicals; hexadecylamine (90%), diphenylphosphine (98%), tri-n-octylphosphine oxide (90%), sulfur (99.998%), octadecene (90%), oleic acid (90%), methanol (99.9%), toluene (99.7%), ethanol (99.9%) were from Sigma Aldrich; 1-dodecylphosphonic acid (98%) was from Epsilon chimie; and oleylamine (80–90%) was from Acros. All chemicals were used as received.

QD Characterization: QDs were characterized by TEM Figure 2b using a Philips CM 12 TEM. Measurements of photoluminescence (PL) spectra in solution are recorded using an Ocean Optics QD65000 spectrometer (see Supporting Information).

Device Fabrication and Characterization: ITO-coated glass received from Thin Film Devices, Annaheim, CA was cleaned and 35 nm of SiO_2 was RF magnetron sputter deposited at 3.0 W cm^{-2} and an Ar pressure of 2×10^{-3} mBar, resulting in a deposition rate of 0.13 Å s^{-1}. QDs solutions with concentrations of 12–20 mg mL^{-1} were spun for 60 s at 2000 rmp with an acceleration of 4000 rpm s^{-1}. A SiO_2 layer was deposited on top

of the QD layer using conditions identical to the first layer. A 70 nm thick Al top electrode was deposited through a shadow mask with a rate of 0.07 Å s^{-1} by DC sputtering at 3.0 W cm^{-2} and an Ar pressure of 5×10^{-3} mBar to obtain a device active area of 2.0 mm^2.

Field-Dependent PL Lifetime Measurements: The devices were mounted in a custom-made holder and were excited by a picosecond pulsed laser (Hamamatsu C10196). The luminescence was collected with a streak scope (Hamamatsu C10627). Electric fields were applied using a Agilent 33522A arbitrary waveform generator connected to a Falco Systems WMA-300 high voltage amplifier. A sense capacitor of C_s = 15.3 nF was used and the capacitance of each SiO_2layer was measured to be C_{ox} = 113 nF cm^{-2}. The voltages V_0, V_s (see Figure 2) were recorded using a Rhode & Schwarz RTM1054 oscilloscope. The calculation of field and charge in the QD film is explained in the Supporting Information.

Simulations: Solutions for the lowest energy electron and hole wavefunctions were found using a quantum mechanical solver based on the empirical tight-binding model.[21] The material parameters for CdSe, CdS, and ZnS were obtained from ref. [22,23]. The relative band offsets were selected to match literature values.[31] The crystal was modelled to be defect-free and unstrained with a lattice constant of 5.82 Å .[23] The field values used in the simulation (F_{exc}) were related to the average field across the QD solid (F_{qd}) by $(F_{exc})\ F_{qd} = \frac{\epsilon_{org}}{f_{qd}\epsilon_{org} + (1-f_{qd})\epsilon_{qd}} = 0.45$. This factor was derived from a two-dielectric model as described in the Supporting Information.

Supporting Information

Supporting Information is available from the Wiley Online Library or from the author.

Acknowledgements

The authors thank Prof. Mathieu Luisier for use of the OMEN simulator and helpful discussions. Funding for this project was supported by the Swiss National Science Foundation (SNSF). TEM was performed at the Electron Microscopy ETH Zurich (EMEZ).

Received: October 30, 2012
Revised: December 4, 2012
Published online: January 22, 2013

[1] V. L. Colvin, M. C. Schlamp, A. P. Alivisatos, *Nature* **1994**, *370*, 354.
[2] J. Kwak, W. K. Bae, D. Lee, I. Park, J. Lim, M. Park, H. Cho, H. Woo, D. Y. Yoon, K. Char, S. Lee, C. Lee, *Nano Lett.* **2012**, *12*, 2362.
[3] J. M. Caruge, J. E. Halpert, V. Wood, V. Bulović, M. G. Bawendi, *Nat. Photonics* **2008**, *2*, 247.
[4] J. E. B. Katari, V. L. Colvin, A. P. Alivisatos, *J. Phys. Chem.* **1994**, *98*, 4109.
[5] G. E. Cragg, A. L. Efros, *Nano Lett.* **2010**, *10*, 313.
[6] C. Galland, Y. Ghosh, A. Steinbrück, J. A. Hollingsworth, H. Htoon, V. I. Klimov, *Nat. Commun.* **2012**, *3* 908.
[7] B. N. Pal, Y. Ghosh, S. Brovelli, R. Laocharoensuk, V. I. Klimov, J. A. Hollingsworth, H. Htoon, *Nano Lett.* **2012**, *12*, 331.
[8] D. Bozyigit, V. Wood, Y. Shirasaki, V. Bulovic, *J. Appl. Phys.* **2012**, *111*, 113701.
[9] S. A. Empedocles, M. G. Bawendi, *Science* **1997**, *278*, 2114.
[10] S.-J. Park, S. Link, W. L. Miller, A. Gesquiere, P. F. Barbara, *Chem. Phys.* **2007**, *341*, 169.
[11] H. Huang, A. Dorn, G. P. Nair, V. Bulović, M. G. Bawendi, *Nano Lett.* **2007**, *7*, 3781.
[12] E. Rothenberg, M. Kazes, E. Shaviv, U. Banin, *Nano Lett.* **2005**, *5*, 1581.
[13] M. Jarosz, V. Porter, B. Fisher, M. Kastner, M. Bawendi, *Phys. Rev. B* **2004**, *70*, 195327.
[14] R. Korlacki, R. F. Saraf, S. Ducharme, *Appl. Phys. Lett.* **2011**, *99*, 153112.
[15] A. W. Achtstein, H. Karl, B. Stritzker, *Appl. Phys. Lett.* **2006**, *89*, 061103.
[16] B. Mahler, P. Spinicelli, S. Buil, X. Quelin, J.-P. Hermier, B. Dubertret, *Nat. Mater.* **2008**, *7*, 659.
[17] C. Galland, Y. Ghosh, A. Steinbrück, M. Sykora, J. A. Hollingsworth, V. I. Klimov, H. Htoon, *Nature* **2011**, *479*, 203.
[18] J. F. Wager, P. D. Keir, *Annu. Rev. Mater. Sci.* **1997**, *27*, 223.
[19] C. L. Braun, *J. Chem. Phys.* **1984**, *80*, 4157.
[20] C. Leatherdale, C. Kagan, N. Morgan, S. Empedocles, M. Kastner, M. Bawendi, *Phys. Rev. B* **2000**, *62*, 2669.
[21] M. Luisier, A. Schenk, W. Fichtner, G. Klimeck, *Phys. Rev. B* **2006**, *74*, 205323.
[22] P. Lippens, M. Lannoo, *Phys. Rev. B* **1990**, *41*, 6079.
[23] P. Lippens, M. Lannoo, *Phys. Rev. B* **1989**, *39*, 10935.
[24] S. Brovelli, R. D. Schaller, S. A. Crooker, F. García-Santamaría, Y. Chen, R. Viswanatha, J. A. Hollingsworth, H. Htoon, V. I. Klimov, *Nat. Commun.* **2011**, *2*, 280.
[25] P. Anikeeva, C. Madigan, J. Halpert, M. Bawendi, V. Bulović, *Phys. Rev. B* **2008**, *78*, 085434.
[26] D. E. Gómez, J. van Embden, P. Mulvaney, M. J. Fernée, H. Rubinsztein-Dunlop, *ACS Vano* **2009**, *3*, 2281.
[27] F. García-Santamaría, S. Brovelli, R. Viswanatha, J. A. Hollingsworth, H. Htoon, S. A. Crooker, V. I. Klimov, *Nano Lett.* **2011**, *11*, 687.
[28] A. V. Malko, Y.-S. Park, S. Sampat, C. Galland, J. Vela, Y. Chen, J. A. Hollingsworth, V. I. Klimov, H. Htoon, *Nano Lett.* **2011**, *11*, 5213.
[29] P. Reiss, J. Bleuse, A. Pron, *Nano Lett.* **2002**, *2*, 781.
[30] A. Sahu, M. S. Kang, A. Kompch, C. Notthoff, A. W. Wills, D. Deng, M. Winterer, C. D. Frisbie, D. J. Norris, *Nano Lett.* **2012**, *12*, 2587.
[31] J. Langer, C. Delerue, M. Lannoo, H. Heinrich, *Phys. Rev. B* **1988**, *38*, 7723.